Supplemental document

This is a supplement to a paper that outlines a framework to support post-earthquake building safety and reoccupancy decisions by quantifying the change in building collapse risk following a mainshock earthquake event. The framework includes three modules, which quantify the elevated hazard (M1), the building collapse performance (M2), and the elevated collapse risk (M3). The paper section titled Elevated Hazard Model (M1) descries the Yeo and Cornell (2009) Aftershock Probabilistic Site Hazard Analysis (APSHA) model and shows how it can be combined with conventional PSHA to define an elevated post-earthquake hazard, which dissipates back to a steady state over time. The Damaged Building Collapse Fragilities (M2) and the Elevated Collapse Risk (M3) modules of the paper are described through case studies for an individual building and a parametric study.

While the individual building case study in the main paper only considered a 20-story reinforced concrete frame building, this supplemental document includes the following three buildings (Galvis et al. 2023):

- 20-story building, with fundamental period T = 2.3 seconds
- 8-story building, T = 1.8 seconds,
- 4-story building, T = 0.95 seconds.

The terms in the APSHA model provide a framework for linking aftershock rates with the probability of exceeding shaking intensities, given the occurrence of an aftershock. As such, neither the assumptions in these case studies (nor those of the original case study in Yeo and Cornell 2009) should be seen as constraints on how the model can be used. Similarly, the individual building's collapse fragilities were conditioned on damage indicators that were identified through sequential nonlinear response history analyses (NLRHA) for a 20-story building (Galvis et al. 2023). While the main paper briefly explored these topics, this supplemental document provides further details of the sensitivity studies that were conducted for the following assumptions:

- Ground motion model, GMM,
  - Boore et al. (2014) (BSSA14),
  - Chiou and Youngs (2008) (CY08) with and without the aftershock flag (AF),
- Magnitude to rupture length relationship,
  - Wells and Coppersmith (1994) for strike-slip faults:
    $\log(L) = 0.74M_w - 3.55$,
    where L is the surface rupture length (*SRL*) with stddev = 0.28 *km*,
- Base rate, a, from the equation for the aftershock productivity rate, $\mu(t|m_m)$,
  - Hardebeck et al. (2019) parameters for northern California,
    mean = -2.64 and standard deviation (stddev) = 0.48,
- Duration of interest for the event occurrence rate, Δt.

Table 1. Assumption alternatives for local sensitivity analyses.

Assumption	Case Study	Alternative 1	Alternative 2
GMM	BSSA14	CY08 with AF	CY08 without AF
L	*mean*	*mean + stddev*	*mean - stddev*
a	*mean*	*mean + stddev*	*mean - stddev*
$\boldsymbol{\Delta t}$	*1 month*	*1 week*	*3 days*

To make this supplement a standalone document, some of the text from the main document is repeated here. Unlike the main paper, which has color figures that are legible in grayscale, this document uses grayscale versus color to differentiate between the baseline study of the ain paper versus the alternatives models, respectively. If viewed in grayscale, the two sets of assumptions will appear identical. However, a careful observer will be able to identify which set of lines remains constant between the adjacent figures and thereby recognize the case study assumption.

Building Height

The building height affects the building period, T. Figure 1 shows the impact of T on the $Sa_{avg}(T)$ hazard curves. As in the main document, the colors in the legend correspond to the mainshock magnitude, m_m, while the linestyle corresponds to the type of hazard (elevated, aftershock, and steady state).

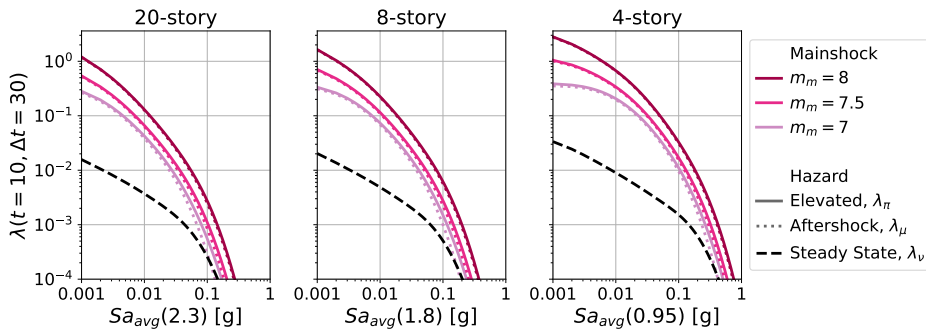

Figure 1. Alternatives for the number of stories in each building.

The elevated collapse risk's sensitivity to T is shown in Figure 2. The alternative assumptions (8-story and 4-story on the left and right, respectively) are shown in the mainshock colors from the legend, as in the main document. The case study's 20-story results are shown in grayscale with the same level saturation, per mainshock magnitude. Note that the risk is quantified as a risk multiplier, or the elevated collapse risk normalized by the steady state (intact, pre-mainshock) collapse risk for each set of assumptions (i.e., even if the absolute value of the steady state risk is greater for one building than for another, they are both shown as unity in the figure.)

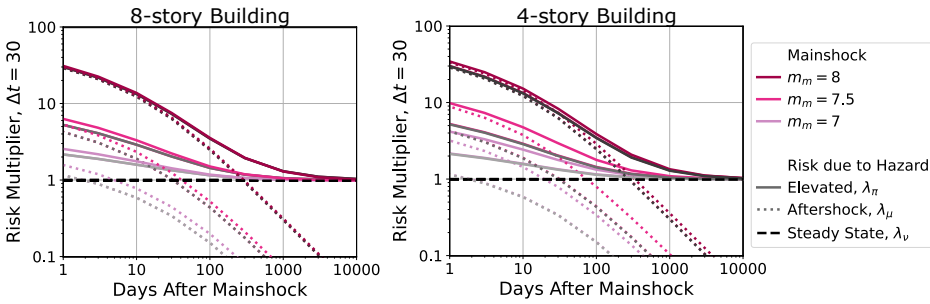

Figure 2. Elevated collapse risk's sensitivity to the building height. The alternative assumptions (8-story and 4-story on the left and right, respectively) are shown in legend's mainshock colors. The case study's 20-story results are shown in grayscale with the same level of saturation.

Note that the elevated risk following the $m_m = 8$ is similar for each building, whereas the risk following the $m_m = 7.5$ and 7 mainshocks increases for shorter buildings (e.g., the 4-story). This is consistent what was seen in Figure 11b of the main document's parametric study, where the risk band for $m_m = 8$ mainshock was relatively insensitive to building period, while the bands for the $m_m = 7$ and 7.5 mainshocks decreased as T increased. This difference is due to the spectral shape of the ground motion model, which is discussed next.

Ground Motion Model

The ground motion model quantifies the the probability of exceeding a shaking intensity, im, given a rupture event of magnitude m, with a site to rupture distance, r, notated as $P(IM > im|m, r)$. Any number of ground motion models (GMMs) could be used to describe this probability distribution. The BSSA14 GMM is one of the models that is used for PSHA of the Western U.S. and has been recently validated for continued use (McNamara et al. 2020). The selected site in downtown San Francisco has an average shear wave velocity over the top 30 m of $V_{s30} = 550$ *m/s* and the fault is assumed to be a vertical strike-slip with ruptures that reach the surface. The BSSA14 GMM uses the Joyner-Boore distance (the closest distance to the surface projection of the fault plane, $R_{jb} = 13\ km$) and does not include the depth to the top of the rupture, Z_{tor}. Figure 3a shows BSSA14's mean predicted spectrum (black line) for a $m = 7$ rupture. The CY08 GMM uses several distance terms, including the distance to the rupture itself, R_{rup}, and Z_{tor}. While the comparisons in this document assume that all ruptures reach the surface, using the CY08 would require an alternate assumption for the depth of the rupture, particularly for small magnitude events.

Recent studies (e.g., Shokrabadi et al. 2018) have suggested using GMMs such as CY08, which includes significant differences in the spectral shape of the mainshock and aftershock ground motions. Differences in spectral shape for the CY08 aftershock model can be seen by comparing the solid and dashed gray lines, respectively in Figure 3a.

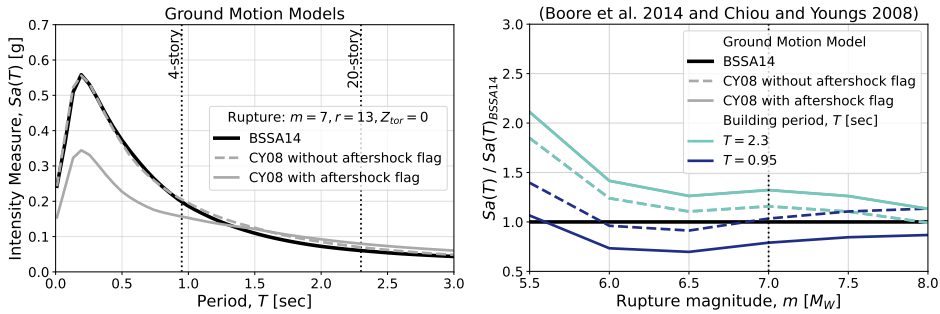

Figure 3. Alternatives for the ground motion model, GMM. **(a)** The case study's BSSA14 is solid black. CY08 (gray) can be used with the aftershock flag (solid) or without (dashed). **(b)** The CY08 $T = 0.95$ and 2.3 spectral accelerations, normalized by BSSA14.

Note that the use of a ground motion model that differentiates between mainshocks and aftershocks would also necessitate an aftershock-specific collapse fragility, due to the influence of the spectral shape on structural response. In contrast, the BSSA14 GMM used in the case study does not include spectral shape differences for aftershock events.

Figure 4 shows the impact of the aftershock flag on the elevated collapse risk for CY08 as compared to BSSA14. Both the 20-story (above) and 4-story (below) results are shown in order to demonstrate the impact of the GMM for tall versus short(er) buildings. The risk multiplier of the 20-story building for CY08 without the aftershock flag (upper left) is slightly higher than the baseline results, particularly for lower-magnitude mainshocks. This can be attributed to CY08 without the aftershock flag's slightly increased predicted mean $Sa(2.3)$ as compared to BSSA14. The increased $Sa(2.3)$ for CY08 without the aftershock flag holds for $m < 8$, as shown by the dashed turquoise in Figure 3b. For aftershock environments following $m_m = 7$ or 7.5 mainshock, the aftershock magnitude upper bound of $m_u = m_m$ results in consistently larger aftershock intensities for CY08 than for BSSA14. For the 4-story building (bottom left of Figure 4), however, the $Sa(0.95)$ intensities for CY08 without the aftershock flag (corresponding to the blue dashed line on Figure 3b) is roughly centered that of BSSA14 for $6 < m < 8$, resulting in roughly equal elevated risk following all three mainshocks. (While the blue dashed line of Figure 3b does increase for $m < 6$, recall from the main document's Figure 3a that the magnitude distribution following each event is identical for $m < 6$, such that any differences between the aftershock hazards following each mainshock are driven by $m > 6$ events.) When using the CY08 aftershock flag (on the right for Figure 4), the relative risk impacts for the 20- versus 4-story buildings are reversed, due to the shift in the $Sa(2.3)$ and $Sa(0.95)$ mean values (solid gray and colored lines in Figure 3a). When using the aftershock flag, the 20-story building's CY08 results are higher than the BSSA14, while the 4-story building's CY08 results are lower, due to the spectral shape associated with the aftershock flag.

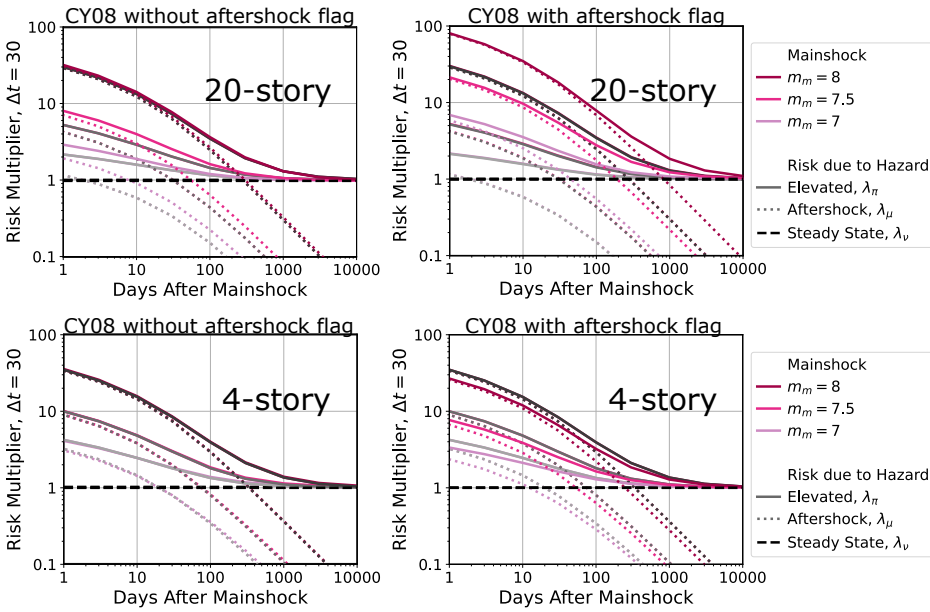

Figure 4. Elevated collapse risk's sensitivity to the ground motion model, GMM. The upper figures are for the case study's 20-story building while the lower figures are for the 4-story building. The CY08 GMM without and with the aftershock flag are on the left and right, respectively.

Magnitude to Rupture Length Relationship

The aftershock rupture length determines the distribution of rupture distances for given magnitude, due to assumption that the entire aftershock rupture fits within the mainshock rupture surface. The case study uses the Wells and Coppersmith (1994) mean of the magnitude to surface rupture length (*SRL*) relationship (solid black in Figure 5). The solid dashed and dash-dot lines are +/-1 standard deviation, respectively. The set of gray lines represents the relationship for the subsurface rupture length (*RLD*). If the RDL definition had been used, the rupture length would increase for $m < 8$.

The elevated collapse risk's sensitivity to the rupture length is shown in Figure 6. The longer lengths ($mean + stddev$ on the left) result in higher risk, especially for higher magnitude mainshocks, as the aftershock rupture's longer length draws them closer to the site, even at the extreme ends of the mainshock rupture surface. (The *RLD* relationship's longer rupture lengths would have the same effect.) The shorter lengths ($mean - stddev$ on the right) result in lower risk, especially for higher magnitude mainshocks.

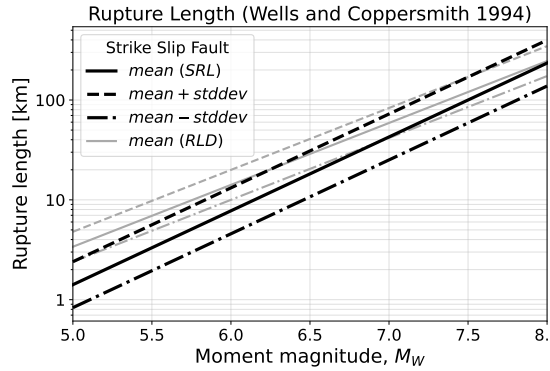

Figure 5. Alternatives for the rupture length, L. The case study uses the mean for the surface rupture length (*SRL*) (solid black line). The black dashed and dash-dot lines are +/-1 standard deviation for the *SRL*. Wells and Coppersmith (1994) also provide a relationship for the subsurface rupture length (*RLD*) (gray lines).

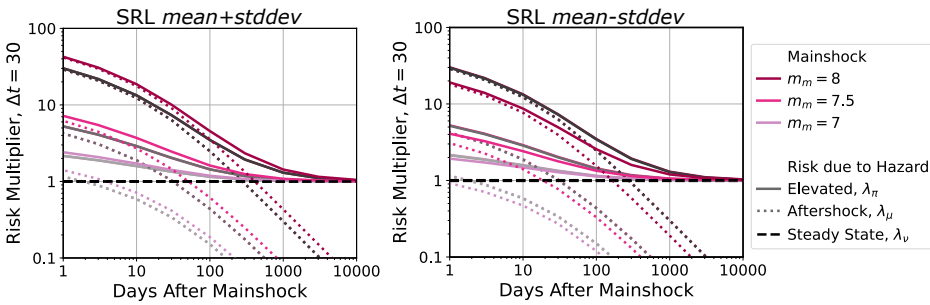

Figure 6. Elevated collapse risk's sensitivity to the surface rupture length, *SRL*.

Aftershock Productivity Base Rate

The rate of aftershock occurrence term, $\mu(t, \Delta t\,|m_m)$, refers to the mean rate of aftershocks following a mainshock magnitude, m_m, during a time window of interest, τ, starting at time t and lasting Δt days, per Equation 1.

$$\mu(t, \Delta t\,|m_m) = \int_t^{t+\Delta t} \mu(\tau|m_m)d\tau =$$

$$\frac{10^{a+b(m_m-m_l)} - 10^a}{p-1}[(t+c)^{1-p} - (t+\Delta t+c)^{1-p}] \quad (1)$$

Hardebeck et al. (2019) provide region-specific values for all the parameters, which are defined in the main document. The focus here is on the base rate, a. For northern

California, the mean value is $a = -2.64$, resulting in the solid black line in Figure 7. The sensitivity of the aftershock rate to variability in a is shown as +/-1 standard deviation (0.48), shown in dashed and dash-dot black lines, respectively. This data indicates that variability in aftershock rates can significantly influence the aftershock risk. For comparison, the gray line shows the aftershock rate for southern California, where the mean value is $a = -2.30$.

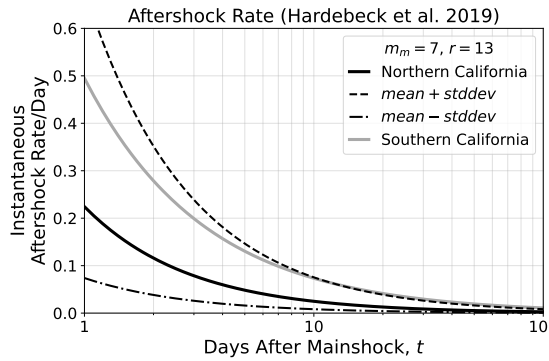

Figure 7. Alternatives for the aftershock model's base rate, a. The case study uses the mean for northern California (solid black line).

The elevated collapse risk's sensitivity to the aftershock base rate is shown in Figure 8. As expected, a higher rate of aftershocks (*mean+stddev* on the left) results in significantly higher risk and vice versa for the lower rate of aftershocks (*mean-stddev* on the right).

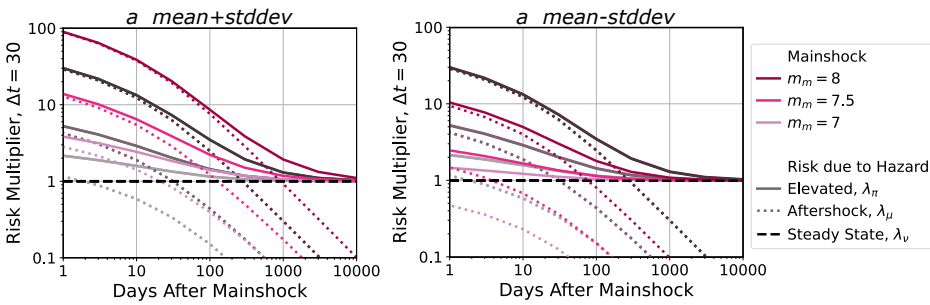

Figure 8. Elevated collapse risk's sensitivity to the aftershock base rate, *a*.

Time Window Duration

The aftershock rate is based on a time window with an assumed duration, Δt. A longer duration starting at the same time, t, after a mainshock will always have more aftershocks. This can be seen in Figure 9, where the case study assumption's 30-day time window

(black line) is higher than the gray lines for shorter time windows. However, the first half of any time window will always have more aftershocks than the second half. Therefore for low start times (e.g., $t < 10\ days$), a shorter time window ($\Delta t_a = 3\ day$) will have a higher mean daily aftershock rate than a longer time window ($\Delta t_b = 1\ month$), i.e., $\mu(t, \Delta t_a)/3\ days > \mu(t, \Delta t_b)/30\ days$. This can be seen by the curves of $\Delta t = 1\ day$ (dotted gray) and $\Delta t = 30\ days$ (solid black) getting close to each other as they approach $t = 0$.

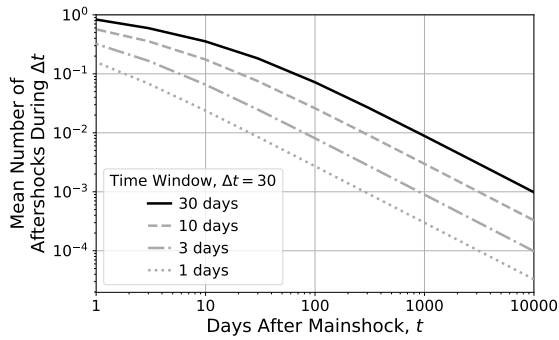

Figure 9. Alternatives for the aftershock model's time window duration, Δt. The case study uses 30 days for the mean monthly rate of aftershock occurrence.

The elevated collapse risk's sensitivity to the time window duration is shown in Figure 10 for $\Delta t = 1\ week$ and $3\ days$. As expected, shorter time windows result in higher risk multipliers while the aftershocks dominate the elevated hazard. The duration of interest should be set based on the type of decision that the analysis is meant to inform.

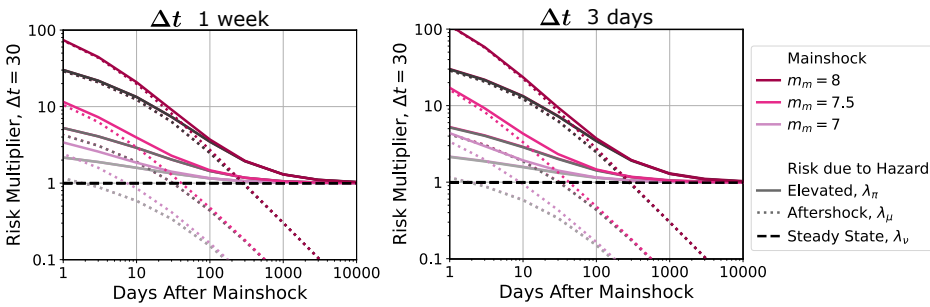

Figure 10. Elevated collapse risk's sensitivity to the time window duration, Δt.

References

Boore DM, Stewart JP, Seyhan E and Atkinson GM (2014) NGA-West2 equations for predicting PGA, PGV, and 5% damped PSA for shallow crustal earthquakes. *Earthquake Spectra* 30(3):

1057–1085. DOI:10.1193/070113EQS184M.

Chiou BSJ and Youngs RR (2008) An NGA Model for the Average Horizontal Component of Peak Ground Motion and Response Spectra. *Earthquake Spectra* 24(1): 173–215. DOI: 10.1193/1.2894832.

Galvis FA, Hulsey AM, Baker JW and Deierlein GG (2023) Simulation-based methodology to identify damage indicators and safety thresholds for post-earthquake evaluation of structures. *Earthquake Engineering & Structural Dynamics* (3): 1–22. DOI:10.1002/eqe.3876.

Hardebeck JL, Llenos AL, Michael AJ, Page MT and van der Elst N (2019) Updated California aftershock parameters. *Seismological Research Letters* 90(1): 262–270. DOI:10.1785/0220180240.

McNamara DE, Wolin EL, Moschetti MP, Thompson EM, Powers PM, Shumway AM, Petersen MD, Wilson DC and Benz HM (2020) Evaluation of ground-motion models for USGS seismic hazard models using near-source instrumental ground-motion recordings of the Ridgecrest, California, earthquake sequence. *Bulletin of the Seismological Society of America* 110(4): 1517–1529. DOI:10.1785/0120200030.

Shokrabadi M, Burton HV and Stewart JP (2018) Impact of Sequential Ground Motion Pairing on Mainshock-Aftershock Structural Response and Collapse Performance Assessment. *Journal of Structural Engineering* 144(10). DOI:10.1061/(ASCE)ST.1943-541X.0002170.

Wells DL and Coppersmith KJ (1994) New empirical relationships among magnitude, rupture length, rupture width, rupture area, and surface displacement. *Bulletin - Seismological Society of America* 84(4): 974–1002.

Yeo GL and Cornell CA (2009) A probabilistic framework for quantification of aftershock ground-motion hazard in California: Methodology and parametric study. *Earthquake Engineering & Structural Dynamics* 38(1): 45–60. DOI:10.1002/eqe.840.